ACS APPLIED ENERGY MATERIALS

www.acsaem.org
Letter

Single Crystalline $Na_{0.67}Ni_{0.33}Mn_{0.67}O_2$ Positive Electrode Material via Molten Salt Synthesis for Sodium Ion Batteries

Jiacheng Hu,[⊥] Qianqian Dou,[⊥] Eric Gabriel, Dewen Hou, Kincaid Graff, Riley Schrock, Mengfei Wu, Shuolei Deng, Joshua A. Russell, Cyrus Koroni, Darin Schwartz, Arwen Zhu, Bryan Li, Yifan Dong,* and Hui Xiong*

Cite This: *ACS Appl. Energy Mater.* 2025, 8, 4941−4947

Read Online

ACCESS | Metrics & More | Article Recommendations | Supporting Information

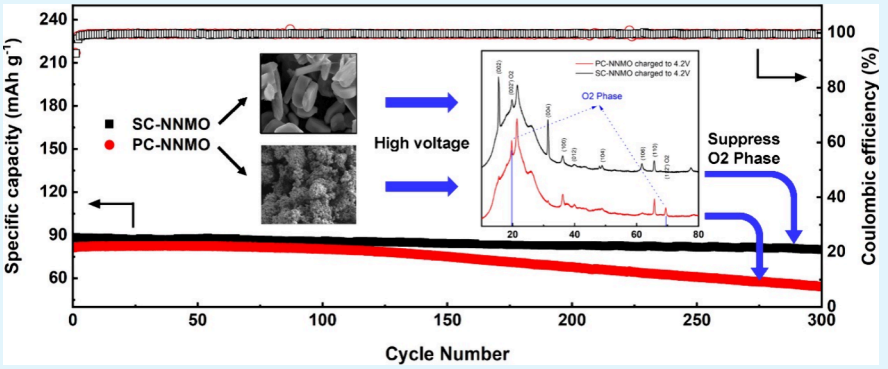

ABSTRACT: P2-layered $Na_{0.67}Ni_{0.33}Mn_{0.67}O_2$ (NNMO) has emerged as a promising positive electrode material for sodium ion batteries due to its appealing electrochemical properties. Synthesis of polycrystalline NNMO (PC-NNMO) materials through conventional calcination of solid precursors remains the prevailing method, where heating occurs in a dry environment with air or O_2. On the other hand, the molten salt method, where precursors are submerged in molten salt medium during calcination, emerged in recent years to be a scalable technique for more controlled crystal growth and uniform morphology in a variety of materials. Here, we utilize the molten salt method to synthesize single crystalline NNMO (SC-NNMO) materials with enhanced electrochemical properties. The SC-NNMO material exhibits an initial specific discharge capacity of 95 mAh g^{-1} at a 0.1C rate, retaining approximately 88.5% of its capacity after 100 cycles over a wide voltage range of 2.0−4.2 V. Furthermore, SC-NNMO maintains a capacity retention of 83.9% after 300 cycles at a 1C rate compared to 66.6% for PC-NNMO, indicating excellent long-term cycling stability. This stability is further confirmed by the performance of an SC-NNMO//hard carbon full cell, which retains 90.3% of its capacity after 200 cycles at 1C within a voltage window of 1.9−4.1 V. The enhancement in stability of the SC-NNMO sample is attributed to the single crystalline structure suppressing the undesired P2−O2 phase transition at high voltage. This study also presents an easy, efficient, and straightforward molten salt process for SC-NNMO material synthesis, offering valuable insights into the potential application of such methodology for the large-scale, cost-effective production of various sodium-layered transition metal oxide positive electrode materials for SIBs.

KEYWORDS: *Molten salt method, Single crystal, Phase transition, layered oxide positive electrode materials, Sodium-ion batteries*

The advancement of large-scale electrochemical energy storage systems has attracted considerable attention in recent years, driven by the growing demand for green and sustainable energy technologies.[1] Among the emerging technologies, sodium-ion batteries (SIBs) have experienced a resurgence of interest as a viable alternative to lithium-ion batteries (LIBs), attributed to their cost-effectiveness, utilization of more abundant and noncritical minerals, and the widespread availability of sodium resources.[2,3] Similar to the positive electrode materials in LIBs, the positive electrode plays a crucial role in determining the overall SIB performance, including capacity, operating voltage, cycle life, and energy density.[4] Among the numerous reported positive electrodes in SIBs, P2-type $Na_{0.67}Ni_{0.33}Mn_{0.67}O_2$ (NNMO) has garnered widespread attention for its exceptional electrochemical performance.[3,5,6] Notably, it exhibits structural stability under ambient conditions, a high average operating voltage, and a

Received: January 28, 2025
Revised: March 30, 2025
Accepted: April 7, 2025
Published: April 10, 2025

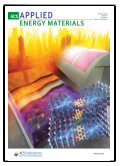

https://doi.org/10.1021/acsaem.5c00264
ACS Appl. Energy Mater. 2025, 8, 4941−4947

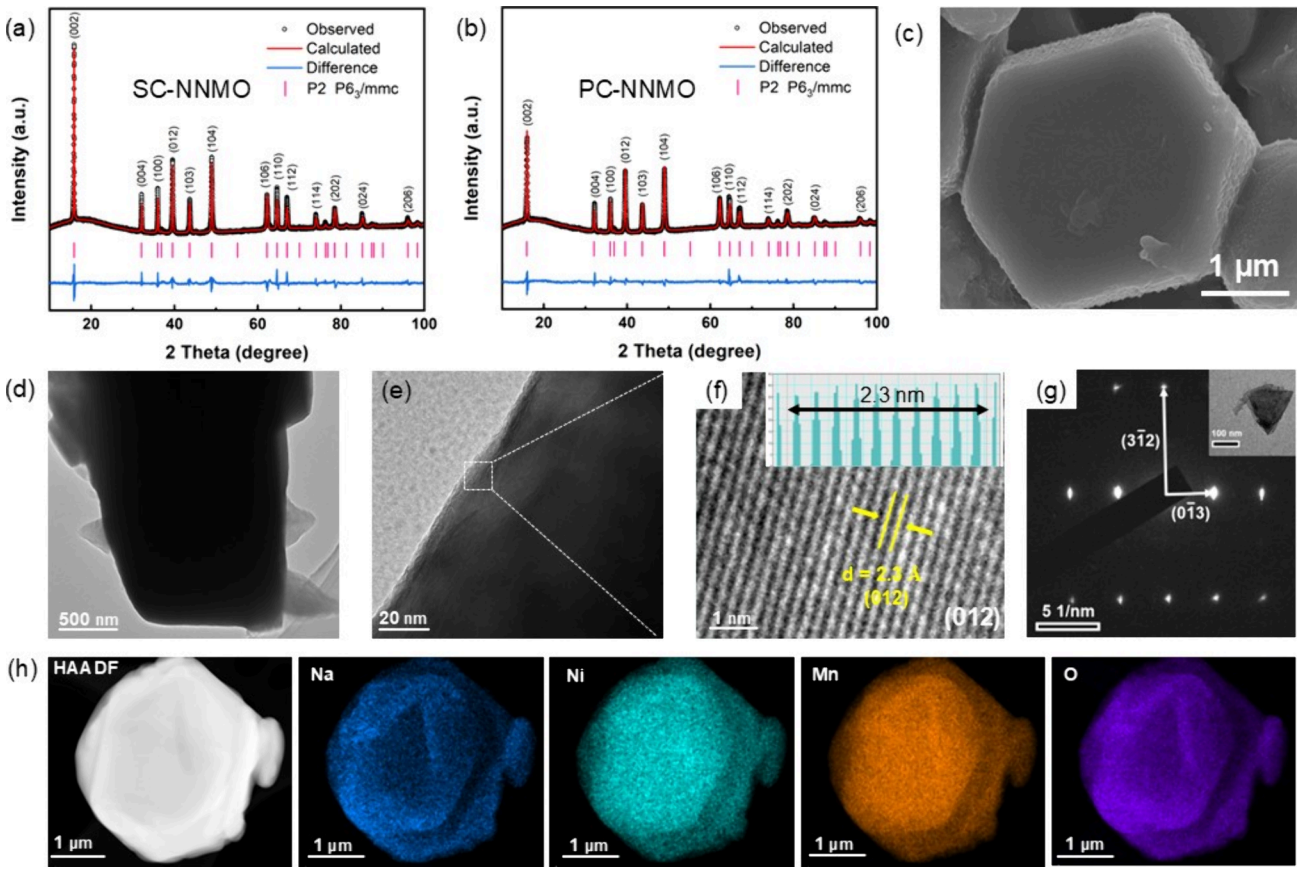

Figure 1. Rietveld refinements of XRD patterns of (a) SC-NNMO and (b) PC-NNMO. (c) SEM image of SC-NNMO. (d) TEM image of SC-NNMO. (e) High-magnification TEM image and (f) HRTEM image of SC-NNMO along the (012) zone axis. (g) Selected area electron diffraction (SAED) pattern of the pristine SC-NNMO sample. (h) High-angle annular dark-field (HAADF) image and corresponding EDS mappings of SC-NNMO.

theoretical capacity of approximately 173 mAh g^{-1}, resulting in the high energy density among layered transition metal oxides when employed in full cell configurations. However, when NNMO is charged to approximately 4.2 V *vs.* Na/Na^+, the removal of Na^+ led to layer glide which induces the P2−O2 phase transition, resulting in rapid capacity degradation.[3,7] In light of the aforementioned challenges affecting the material's cycling stability, optimization strategies have been implemented,[8] including element substitution or doping[5] and surface modification.[9]

The synthesis of NNMO has predominantly yielded polycrystalline secondary particles formed through traditional coprecipitation and calcination methods to date. Interests in obtaining single-crystal materials as a promising alternative to polycrystalline materials has grown in recent years, aiming to address capacity degradation via prioritizing the mitigation of intergranular particle cracking.[10] Various methods have been used for synthesizing single-crystal particles; among them, the molten salt method is especially compelling for its capability to facilitate the dissolution and subsequent recrystallization of active materials during the synthesis process.[11]

The molten salt synthesis utilizes molten salt as a reaction medium for constituent precursors, enabling molecular-scale mixing of reactants and yielding a homogeneous and structurally uniform final product. It is widely regarded as one of the simplest and most cost-effective strategies for fabricating positive electrode materials for LIB systems.[12,13] Despite the similarity in SIB and LIB systems, reports on the synthesis of positive electrode materials using molten salt methods in SIBs remain scarce. Recently, Manthiram's group has reported several studies on the synthesis of single-crystal layered sodium positive electrode materials via the molten salt method, showcasing markedly improved electrochemical performance over conventional polycrystalline counterparts.[10,14] In their experiments, they used NaOH as the Na source to synthesize the material, which involves multiple heating and cooling stages during the calcination process owing to the initial melting of NaOH. Zhao et al. synthesized a high-performance rod-shaped $Na_{0.44}MnO_2$ positive electrode material by the molten salt method.[15] They found this rod-shaped $Na_{0.44}MnO_2$ was generated from Na-birnessite, and this structure showed excellent long-term cycling stability.[15]

Here, we investigate the morphological and structural characteristics and electrochemical performance of single crystalline P2-type NNMO (SC-NNMO) positive electrode material synthesized using a straightforward NaCl-based molten salt method. Na_2CO_3 is used as the Na source, and a simple continuous heating and natural cooling process is adopted to synthesize the single crystal material. Compared to polycrystalline NNMO (PC-NNMO) synthesized by the conventional calcination method, single crystalline NNMO with a plate-like morphology could be made which exhibited an initial capacity of 90.6 mAh g^{-1} at 0.1C between 2.0 and 4.2 V, with a retention of 88.5% after 100 cycles. The material demonstrated long-term stability, retaining 83.9% of its initial capacity after 300 cycles at 1C. In a SC-NNMO//hard carbon

https://doi.org/10.1021/acsaem.5c00264
ACS Appl. Energy Mater. 2025, 8, 4941−4947

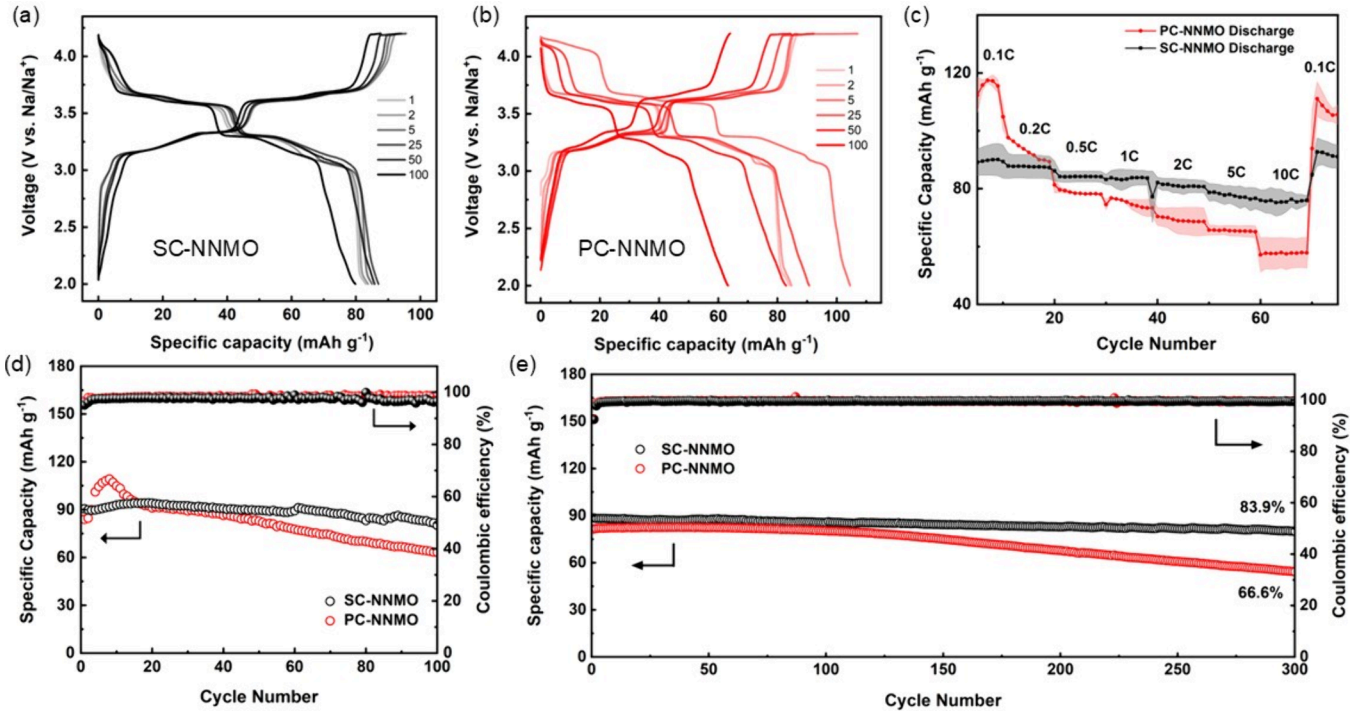

Figure 2. Voltage profiles of (a) SC-NNMO and (b) PC-NNMO at 0.1C rate at different cycles (1C corresponds to 150 mA g^{-1}). (c) Rate capability with standard deviation. Cycle life at (d) 0.1C rate and (e) 1C rate.

full cell, it still retained 90.3% of its initial capacity after 200 cycles at 1C. This work establishes molten salt synthesis as a facile, scalable, and efficient approach for producing high-performance single-crystal positive electrode materials for sodium-ion batteries.

SC-NNMO and PC-NNMO were synthesized via the molten salt and conventional coprecipitation−calcination method, respectively. The conventional coprecipitation−calcination synthesis method was adopted from previous work.[5] The molten salt method is briefly described as follows: Anhydrous ethanol served as the dispersant. NaCl was used as the molten salt flux. NiO, Mn_2O_3, Na_2CO_3, and NaCl were uniformly hand-ground for 20 min in an agate mortar in a molar ratio of 1:1:1.05:2, with ethanol. The extra Na_2CO_3 (5%) was used to account for the loss during high temperature calcination. The mixed powders were then calcined in a furnace at 1000 °C for 15 h under air, followed by natural cooling to room temperature. The final product was then transferred to a glovebox to prevent air exposure. Details of the material characterization and electrochemical testing are provided in the experimental section in the Supporting Information.

The crystal structure of as-synthesized samples was characterized by X-ray diffraction (XRD, Figure 1a and b). No impurities or secondary phases were observed in these two samples. SC-NNMO showed highly intense and sharp peaks, while PC-NNMO showed less intense and broader diffraction peaks.[16] Both samples displayed well-indexed diffraction patterns consistent with the Na_xCoO_2-type P2 structure (space group: $P6_3/mmc$), as determined by Rietveld refinement, and the refined results are presented in Tables S1 and S2. The atomic ratios of Na, Ni, and Mn in the as-prepared samples were determined via inductively coupled plasma mass spectrometry (ICP-MS) measurement and found to be 0.65, 0.34, and 0.66 for SC-NNMO and 0.68, 0.33, and 0.67 for PC-NNMO (Table S3), closely aligning with the target composition of Na, Ni, and Mn, except for the slightly lower Na content in SC-NNMO. The reduction in Na content of SC-NNMO was due to the sodium loss/evaporation during the high temperature calcination process.

The morphologies of SC-NNMO and PC-NNMO samples were investigated using a scanning electron microscope (SEM), shown in Figure S1 and Figure S2. The SC-NNMO sample exhibits an average particle size of approximately 3 μm, demonstrating a plate-like morphology, while the PC-NNMO sample is composed of ∼10 μm secondary particles with densely packed primary particles. The plate-like morphology of SC-NNMO is also shown in Figure 1c. The microstructure of SC-NNMO particles was further examined by using high-resolution transmission electron microscopy (HRTEM). The SC-NNMO material exhibited a single crystal structure, consistent with the XRD patterns (Figure 1d−g). The interplanar spacing was determined to be 0.23 nm, corresponding to the (012) diffraction plane of the P2-type structure. Additionally, energy-dispersive X-ray spectroscopy (EDS) mappings in Figure 1h verified that all elements were uniformly distributed.

The electrochemical performances of SC-NNMO and PC-NNMO electrode materials were evaluated in a Na half-cell configuration within 2.0−4.2 V *vs.* Na/Na^+. Figure 2a and b shows the voltage profiles of the two samples in different cycles. A series of plateaus at distinct voltage ranges were observed during the initial cycle, corresponding to various redox reactions and the rearrangement of Na^+/vacancy ordering.[6,17] When the SC-NNMO positive electrode material charged to the voltage around 4.2 V, the shorter voltage plateau (compared to PC-NNMO) demonstrated better stability at high voltage, owing to the suppression of P2−O2 phase transition. Figure 2c compares the rate capabilities of the two samples, showing the SC-NNMO sample exhibiting

https://doi.org/10.1021/acsaem.5c00264
ACS Appl. Energy Mater. 2025, 8, 4941−4947

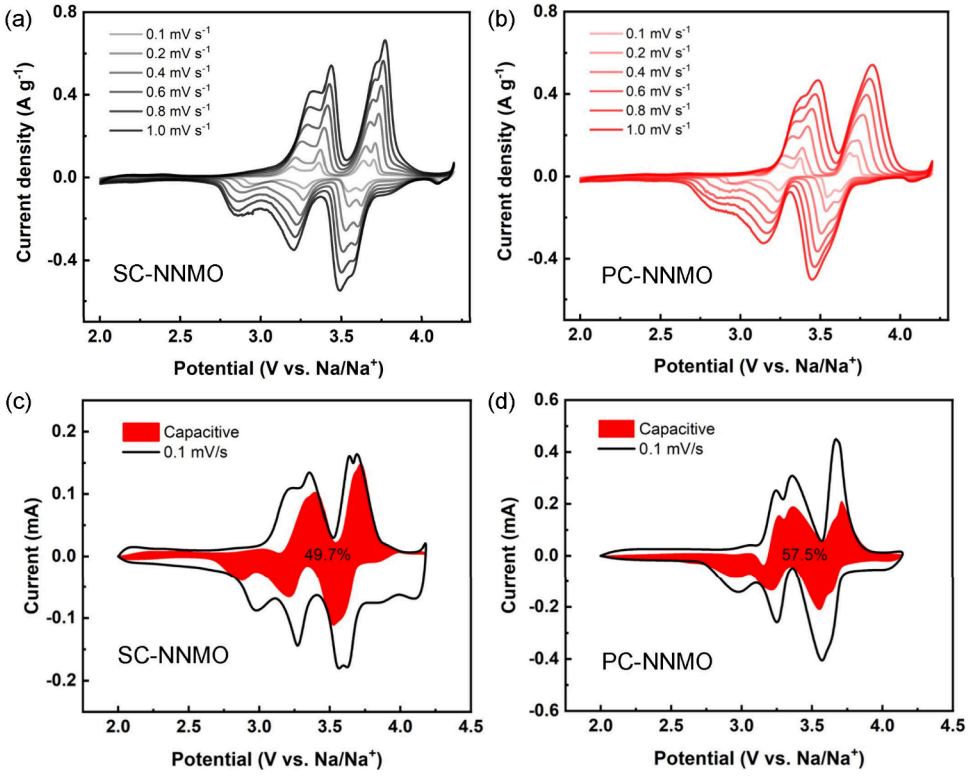

Figure 3. Cyclic voltammograms of (a) SC-NNMO and (b) PC-NNMO positive electrode materials at different scan rates and the voltametric response for (c) SC-NNMO and (d) PC-NNMO at 0.1 mV s^{-1}. The red shaded area is the capacitive contribution.

superior performance. The average discharge capacities of SC-NNMO were 84.4, 83.6, 82.3, 79.5, 78.8, 74.3, and 72.3 mAh g^{-1} at 0.1C, 0.2C, 0.5C, 1C, 2C, 5C, and 10C, respectively. The observed capacity of the PC-NNMO electrode increased in the first ten cycles, possibly due to the initial insufficient wetting of the electrode−electrolyte interface.[15] Upon returning to 0.1C from the 10C rate, the capacity fully recovered, indicating rapid kinetics for the SC-NNMO positive elelctrode.[18] However, the rate capacities of PC-NNMO displayed a faster decline with an increasing C rate. The cycling stability of the two samples at a low C rate (0.1C) and a high C rate (1C) is shown in Figure 2d and e, respectively. The initial specific discharge capacity of SC-NNMO at 0.1C was 90.6 mAh g^{-1}, with a capacity retention rate reaching 88.5% after 100 cycles, while the PC-NNMO was only 75.6%. Furthermore, at a high C rate (1C), the capacity retention for SC-NNMO was 83.9% compared to 66.6% for PC-NNMO after 300 cycles, with an average Coulombic efficiency exceeding 95% (Figure 2e). The excellent cycling performance of SC-NNMO suggested that NNMO synthesized via the molten salt method exhibited superior structural stability.

In order to understand the Na^+ storage mechanism in the samples, a cyclic voltammetry (CV) measurement with varying scan rates was conducted. First, the CV curves of the SC-NNMO sample at a scan rate of 0.1 mV s^{-1} during the initial cycle (Figure S3(a)) exhibited four redox peak pairs at 3.70/3.60 (~100 mV of peak separation), 3.65/3.54 (90 mV), 3.36/3.26 (100 mV), and 3.25/2.97 V (280 mV), respectively. These peak pairs correspond to the plateaus appearing in the initial cycle (Figure 2a). Similarly, the PC-NNMO electrode material also showed four pairs of redox peaks as shown in Figure S3(b) at 3.73/3.60 (130 mV), 3.69/3.54 (150 mV), 3.39/3.24 (150 mV), and 3.31/2.97 V (340 mV). Both samples displayed four distinctive redox peaks pairs, near ~3.1, 3.3, 3.6, and 3.7 V *vs.* Na/Na^+ associated with $Ni^{2+/3+/4+}$ redox, which was consistent with results reported in the literature[19] and indicating these two samples had undergone similar redox reactions. The lower peak separation of the SC-NNMO sample suggested it has lower polarization and higher reversibility. Besides, the high degree of overlap between the second and the third cycles of SC-NNMO indicated a highly reversible Na^+ insertion and extraction process.[20] Thus, the SC-NNMO electrode material demonstrated superior reversibility compared to that of the PC-NNMO electrode material. Additionally, the little deviation observed in first three cycles may be associated with side reactions, such as surface interactions between the electrolyte and electrodes.[15]

The CV curves of SC-NNMO and PC-NNMO samples at different scan rates are shown in Figure 3a and b. The corresponding CV responses could be analyzed based on the analysis equation,[21,22] $i(V) = k_1\nu + k_2\nu^{1/2}$, where the terms $k_1\nu$ and $k_2\nu^{1/2}$ refer to the contributions from surface capacitive and diffusion-controlled intercalation, respectively. It was found that the capacitive contribution of the SC-NNMO sample (Figure 3c) was 49.7%, a little lower than 57.5% of the PC-NNMO (Figure 3d) at 0.1 mV s^{-1}, which is reasonable since SC-NNMO has a smaller surface area. This suggests that there is more diffusion contribution in the SC-NNMO sample than PC-NNMO.

The electrochemical impedance spectroscopy (EIS) measurements for both samples were then conducted to investigate pristine and cycled samples' Na^+ diffusion kinetics. The Nyquist plots and the corresponding equivalent circuit of pristine and cycled samples, employed to model the interfacial properties, are shown in Figure S4a and b. Both samples exhibited two semicircles in the intermediate frequency region

https://doi.org/10.1021/acsaem.5c00264
ACS Appl. Energy Mater. 2025, 8, 4941−4947

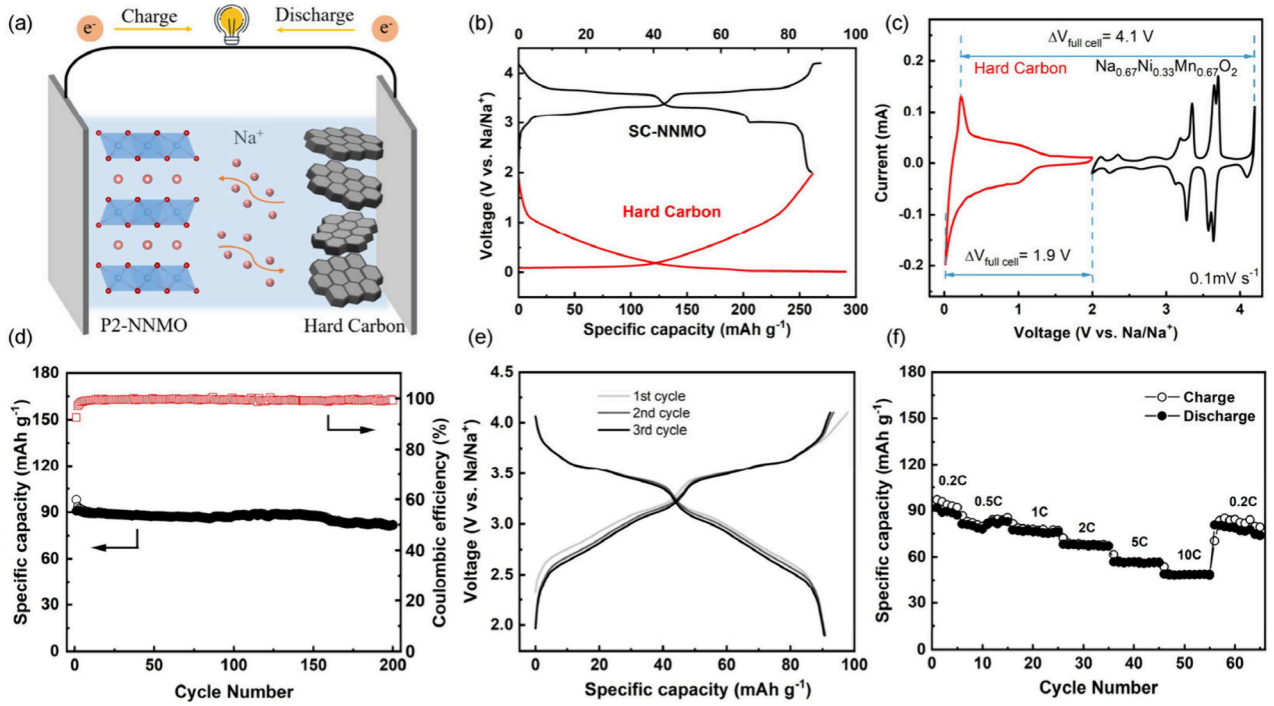

Figure 4. (a) Schematic diagram of Na ion full batteries with SC-NNMO and hard carbon electrode material. (b) Voltage profiles and (c) CV curves of SC-NNMO positive electrode material and hard carbon negative electrode materials. (d) Cycling performance at 1C (based on the active mass positive electrode). (e) Voltage profiles and (f) rate capabilities of the full battery at 1.9−4.1 V.

and an oblique line in the low frequency region, which correspond to the ohmic resistance ($R\Omega$) at the intercept, cathode electrolyte interphase resistance (R_{SEI}), charge transfer resistance (R_{ct}), and Warburg impedance (Z_w), respectively. The R_{ct} represents the Na^+ charge transfer resistance at the interface between the electrode and the electrolyte,[23] while Z_w is associated with Na^+ diffusion within the bulk of the electrode materials.[24] It was observed that the pristine PC-NNMO electrode material exhibited a higher R_{ct} (752.7 Ω) value compared to pristine SC-NNMO (309.1 Ω), indicating more grain boundaries for polycrystalline PC-NNMO might impede the charge transfer kinetics at the electrode/electrolyte interface.[23] The EIS of both samples after the 10th cycle is shown in Figure S4b. Both electrodes exhibited reduced impedance, which suggested activation of the electrodes during cycling. It was evidenced that SC-NNMO exhibited a lower R_{ct} (233.3 Ω) compared to PC-NNMO (295.5 Ω). The lower R_{ct} in the SC-NNMO electrode material can be attributed to its superior structural stability by suppressing the P2−O2 phase transition around 4.2 V (ex situ XRD, Figure S5), which also agrees with the shorter plateau in Figure 2b. Meanwhile, the crystal structures and morphologies of SC-NNMO and PC-NNMO samples cycled after 200 cycles at 0.1C were examined. XRD results (Figure S6) suggest that both samples maintained the P2 structure. On the other hand, the cycled PC-NNMO electrode exhibited a large number of cracks as compared to the SC-NNMO electrode (Figure S7), which indicates the improved mechanical properties of the SC-NNMO material. In addition, the Na^+ diffusion coefficients for SC-NNMO and PC-NNMO can be calculated through EIS (Note S1 in Supporting Information, Figure S4c) and were 4.07×10^{-11} and 4.37×10^{-12} m s^{-1}, respectively. The one magnitude higher value of the Na^+ diffusion coefficient indicated the faster kinetic behavior of SC-NNMO than the PC-NNMO sample, which corroborates well with the rate performance.

A full cell featuring the SC-NNMO positive and commercial hard carbon (HC) negative electrode material (denoted as SC-NNMO//HC) was assembled into a coin-type battery. Prior to assembling the full cell, the HC negative electrode was precycled in a half cell at 0.1C for three cycles to enhance its initial Coulombic efficiency (Figure S8). The reaction mechanism of the charge−discharge process is schematically illustrated in Figure 4a. During the charging process, Na^+ was extracted from the SC-NNMO side and inserted into the HC side, while electrons migrated through the external circuit to the negative electrode material and vice versa. Figure 4b and c shows the voltage profiles and CV curves of SC-NNMO and HC. Figure 4e presents the galvanostatic charge−discharge curves of the coin-type full cell battery, demonstrating a specific capacity of approximately 100 mAh g^{-1} based on the positive electrode material mass at 1.9−4.1 V. Figure 4f illustrates the electrochemical performance of the SC-NNMO//HC coin-type full cell at various current densities, delivering specific capacities of 112.2, 81.2, 77.4, 68.3, 56.9, and 49.1 mAh g^{-1} at discharge rates of 0.2 0.5, 1, 2, 5, and 10 C, respectively. A Ragone plot based on the total mass of both positive and negative materials is presented in Figure S9 to compare the power density vs energy density. Cycling performance in the full cell was a critical indicator for commercialization; thus, the cycling stability of the SC-NNMO//HC coin-type full cell was evaluated following the rate capability test, as shown in Figure 4d. This coin-type full cell exhibited a good capacity retention of 89.7% after 200 cycles at 1C.

In conclusion, single crystalline $Na_{0.67}Ni_{0.33}Mn_{0.67}O_2$ positive electrode material with an average particle size of ∼3 μm can be synthesized by a simple molten salt method. The

https://doi.org/10.1021/acsaem.5c00264
ACS Appl. Energy Mater. 2025, 8, 4941−4947

composition, morphology, and structure were determined by ICP-MS, XRD, SEM, and TEM characterization. Compared to polycrystalline NNMO synthesized via the conventional coprecipitation−calcination method, SC-NNMO demonstrated superior structural stability and fast kinetics as indicated by excellent long cycling stability and rate capability in the wide voltage range of 2.0−4.2 V. The enhancement in cycling stability of the SC-NNMO sample can be explained by the suppressed P2−O2 phase transition at high voltage, which was further proven by ex situ XRD results. The Na^+ charge storage and transport kinetics of the SC-NNMO and PC-NNMO electrode materials were evaluated by CV and EIS. It was found that the SC-NNMO sample has the higher capacity at a high C rate and good rate capability, which can be ascribed to its high Na^+ diffusivity. Analysis of the capacitive and diffusion contribution in Na^+ charge storage of the SC-NNMO sample suggests that there is more contribution from diffusion-limited intercalation for a single crystal structure than a polycrystalline structure. Moreover, inspired by the outstanding performance observed in half-cell testing, a full cell using the SC-NNMO and commercial HC electrode materials was assembled in a coin-type configuration. This full cell also exhibited an impressive capacity retention, demonstrating its significant practicality. This work offered a new strategy in synthesizing high-performance layered oxide positive electrode materials via the molten salt method for sodium-ion batteries.

■ ASSOCIATED CONTENT

Data Availability Statement

The data that support the findings of this study are available upon request.

Supporting Information

The Supporting Information is available free of charge at https://pubs.acs.org/doi/10.1021/acsaem.5c00264.

Experimental section, SEM images, CV, EIS, XRD patterns, ICP-MS data, and additional electrochemistry data (PDF)

■ AUTHOR INFORMATION

Corresponding Authors

Hui Xiong − *Micron School of Materials Science and Engineering, Boise State University, Boise, Idaho 83720, United States;* orcid.org/0000-0003-3126-1476; Email: clairexiong@boisestate.edu

Yifan Dong − *Micron School of Materials Science and Engineering, Boise State University, Boise, Idaho 83720, United States*; Email: dyfdongyifan@gmail.com

Authors

Jiacheng Hu − *Micron School of Materials Science and Engineering, Boise State University, Boise, Idaho 83720, United States*

Qianqian Dou − *Faculty of Materials Science and Chemistry, China University of Geosciences, Wuhan 430070, P. R. China*

Eric Gabriel − *Micron School of Materials Science and Engineering, Boise State University, Boise, Idaho 83720, United States;* orcid.org/0000-0002-1026-2413

Dewen Hou − *Micron School of Materials Science and Engineering, Boise State University, Boise, Idaho 83720, United States; Center for Nanoscale Materials, Argonne National Laboratory, Lemont, Illinois 60439, United States*

Kincaid Graff − *Micron School of Materials Science and Engineering, Boise State University, Boise, Idaho 83720, United States*

Riley Schrock − *Micron School of Materials Science and Engineering, Boise State University, Boise, Idaho 83720, United States*

Mengfei Wu − *Faculty of Materials Science and Chemistry, China University of Geosciences, Wuhan 430070, P. R. China*

Shuolei Deng − *Faculty of Materials Science and Chemistry, China University of Geosciences, Wuhan 430070, P. R. China*

Joshua A. Russell − *Micron School of Materials Science and Engineering, Boise State University, Boise, Idaho 83720, United States*

Cyrus Koroni − *Micron School of Materials Science and Engineering, Boise State University, Boise, Idaho 83720, United States*

Darin Schwartz − *Department of Geosciences, Boise State University, Boise, Idaho 83720, United States*

Arwen Zhu − *Micron School of Materials Science and Engineering, Boise State University, Boise, Idaho 83720, United States*

Bryan Li − *Micron School of Materials Science and Engineering, Boise State University, Boise, Idaho 83720, United States*

Complete contact information is available at: https://pubs.acs.org/10.1021/acsaem.5c00264

Author Contributions

⊥J.H. and Q.D. contributed equally. Y.D. and H.X. conceived and designed all experiments. J.H., E.G., K.G., A.Z., and B.L. synthesized $Na_{0.67}Ni_{0.33}Mn_{0.67}O_2$ materials by the conventional coprecipitation−calcination method. J.H., Q.D., R.S., M.W., and S.D. synthesized single crystalline $Na_{0.67}Ni_{0.33}Mn_{0.67}O_2$ materials via the molten salt method. J.H. and Q.D. performed electrochemical measurements. J.H. and J.A.R. collected and analyzed XRD data. J.H. and Q.D. carried out the SEM experiment. D.H., C.K., and S.D. performed TEM test. D.S. carried out the ICP-MS experiment. J.H., Y.D., and H.X. drafted and revised the manuscript. All authors discussed the experimental results and coedited the manuscript.

Notes

The authors declare no competing financial interest.

■ ACKNOWLEDGMENTS

This material is based upon work supported by the U.S. Department of Energy, Office of Science, Office of Basic Energy Sciences program under Award Number DE-SC0024404. K. Graff and C. Koroni acknowledge the support by U.S. National Science Foundation (NSF) (Grant No. DUE-2111549). This research used resources of the Center for Nanoscale Materials, a DOE Office of Science User Facility operated for the DOE Office of Science by Argonne National Laboratory under Contract DE-AC02-06CH11357. This research utilized the XRD, SEM, and TEM instruments in the Boise State University FaCT Core Facility, RRID: SCR_024733, which receives support from the National Institutes of Health [NIH] under the Institutional Development Awards [IDeA] Program of the National Institute of General Medical Sciences [NIGMS] via Grants P20GM148321 and P20GM103408. Funding for the analytical infrastructure of the Boise State Isotope Geology Laboratory

used in this study was provided by NSF Grants EAR-1735889 and EAR-1920336.

REFERENCES

(1) Khan, M. K.; Raza, M.; Shahbaz, M.; Farooq, U.; Akram, M. U. Recent Advancement in Energy Storage Technologies and Their Applications. *J. Energy Storage* **2024**, *92*, No. 112112.
(2) Zuo, W.; Innocenti, A.; Zarrabeitia, M.; Bresser, D.; Yang, Y.; Passerini, S. Layered Oxide Cathodes for Sodium-Ion Batteries: Storage Mechanism, Electrochemistry, and Techno-Economics. *Acc. Chem. Res.* **2023**, *56* (3), 284−296.
(3) Chang, L.; Yang, R.; Bi, X.; Yang, W.; Cai, K.; Wei, A.; Liu, J. Research Progress of Layered P2-Na2/3Ni1/3Mn2/3O2 Cathode Material for Sodium Ion Batteries. *J. Energy Storage* **2023**, *73*, No. 109025.
(4) Yabuuchi, N.; Kubota, K.; Dahbi, M.; Komaba, S. Research Development on Sodium-Ion Batteries. *Chem. Rev.* **2014**, *114* (23), 11636−11682.
(5) Xie, Y.; Gabriel, E.; Fan, L.; Hwang, I.; Li, X.; Zhu, H.; Ren, Y.; Sun, C.; Pipkin, J.; Dustin, M.; Li, M.; Chen, Z.; Lee, E.; Xiong, H. Role of Lithium Doping in P2-Na $_{0.67}$ Ni $_{0.33}$ Mn $_{0.67}$ O $_{2}$ for Sodium-Ion Batteries. *Chem. Mater.* **2021**, *33* (12), 4445−4455.
(6) Gabriel, E.; Wang, Z.; Singh, V. V.; Graff, K.; Liu, J.; Koroni, C.; Hou, D.; Schwartz, D.; Li, C.; Liu, J.; Guo, X.; Osti, N. C.; Ong, S. P.; Xiong, H. Influence of Interlayer Cation Ordering on Na Transport in P2-Type Na $_{0.67-x}$ Li $_{y}$ Ni $_{0.33-z}$ Mn $_{0.67+z}$ O_2 for Sodium-Ion Batteries. *J. Am. Chem. Soc.* **2024**, *146* (22), 15108−15118.
(7) Xu, J.; Lee, D. H.; Clement, R. J.; Yu, X. Q.; Leskes, M.; Pell, A. J.; Pintacuda, G.; Yang, X. Q.; Grey, C. P.; Meng, Y. S. Identifying the Critical Role of Li Substitution in P2-Na-x LiyNizMn1-y-z O-2 (0 < x, y, *z* < 1) Intercalation Cathode Materials for High-Energy Na-Ion Batteries. *Chem. Mater.* **2014**, *26* (2), 1260−1269.
(8) Peng, B.; Wan, G.; Ahmad, N.; Yu, L.; Ma, X.; Zhang, G. Recent Progress in the Emerging Modification Strategies for Layered Oxide Cathodes toward Practicable Sodium Ion Batteries. *Adv. Energy Mater.* **2023**, *13* (27), No. 2300334.
(9) Liu, Y.; Fang, X.; Zhang, A.; Shen, C.; Liu, Q.; Enaya, H. A.; Zhou, C. Layered P2-Na2/3[Ni1/3Mn2/3]O2 as High-Voltage Cathode for Sodium-Ion Batteries: The Capacity Decay Mechanism and Al2O3 Surface Modification. *Nano Energy* **2016**, *27*, 27−34.
(10) Darga, J.; Manthiram, A. Facile Synthesis of O3-Type NaNi $_{0.5}$ Mn $_{0.5}$ O $_{2}$ Single Crystals with Improved Performance in Sodium-Ion Batteries. *ACS Appl. Mater. Interfaces* **2022**, *14* (47), 52729−52737.
(11) Burke, S.; Whitacre, J. Using Molten-Salts as a Thermal Processing Medium for Cobalt-Free Lithium-Rich Cathode Material. *Electrochem. Commun.* **2023**, *157*, No. 107617.
(12) ZhenYao, W.; Biao, L.; Jin, M.; DingGuo, X. Molten Salt Synthesis and High-Performance of Nanocrystalline Li-Rich Cathode Materials. *RSC Adv.* **2014**, *4* (30), 15825.
(13) Chang, Z.; Chen, Z.; Wu, F.; Tang, H.; Zhu, Z.; Yuan, X.; Wang, H. Synthesis and Properties of High Tap-Density Cathode Material for Lithium Ion Battery by the Eutectic Molten-Salt Method. *Solid State Ion.* **2008**, *179* (39), 2274−2277.
(14) Darga, J.; Manthiram, A. Deconstructing the High Voltage Degradation Mechanisms in Na $_{2/3}$ Ni $_{1/3}$ Mn $_{2/3}$ O $_{2}$ with Single Crystals and Advanced Electrolyte. *Adv. Funct. Mater.* **2024**, *34*, No. 2408642.
(15) Zhao, H.; Wu, L.; Tian, J.; Zhang, D.; Li, X.; Xu, S.; Chen, L.; Yi, Q.; Dai, K.; Guo, H. Molten-Salt Assisted Synthesis of a High-Performance Oxide Cathode for Sodium-Ion Batteries: $Na_{0.44}$ MnO_2 as a Case. *New J. Chem.* **2023**, *47* (8), 3892−3902.
(16) Weber, R.; Fell, C. R.; Dahn, J. R.; Hy, S. Operando X-Ray Diffraction Study of Polycrystalline and Single-Crystal Li_x $Ni_{0.5}$ $Mn_{0.3}$ $Co_{0.2}$ O_2. *J. Electrochem. Soc.* **2017**, *164* (13), A2992−A2999.
(17) Lee, D. H.; Xu, J.; Meng, Y. S. An Advanced Cathode for Na-Ion Batteries with High Rate and Excellent Structural Stability. *Phys. Chem. Chem. Phys.* **2013**, *15* (9), 3304−3312.
(18) Heubner, C.; Nikolowski, K.; Reuber, S.; Schneider, M.; Wolter, M.; Michaelis, A. Recent Insights into Rate Performance Limitations of Li-ion Batteries. *Batter. Supercaps* **2021**, *4* (2), 268−285.
(19) Mao, J.; Liu, X.; Liu, J.; Jiang, H.; Zhang, T.; Shao, G.; Ai, G.; Mao, W.; Feng, Y.; Yang, W.; Liu, G.; Dai, K. P2-Type $Na_{2/3}$ $Ni_{1/3}$ $Mn_{2/3}$ O_2 Cathode Material with Excellent Rate and Cycling Performance for Sodium-Ion Batteries. *J. Electrochem. Soc.* **2019**, *166* (16), A3980−A3986.
(20) Shi, S. J.; Tu, J. P.; Tang, Y. Y.; Liu, X. Y.; Zhao, X. Y.; Wang, X. L.; Gu, C. D. Morphology and Electrochemical Performance of Li[Li0.2Mn0.54Ni0.13Co0.13]O2 Cathode Materials Treated in Molten Salts. *J. Power Sources* **2013**, *241*, 186−195.
(21) Costentin, C.; Porter, T. R.; Savéant, J.-M. How Do Pseudocapacitors Store Energy? Theoretical Analysis and Experimental Illustration. *ACS Appl. Mater. Interfaces* **2017**, *9* (10), 8649−8658.
(22) Wang, J.; Polleux, J.; Lim, J.; Dunn, B. Pseudocapacitive Contributions to Electrochemical Energy Storage in TiO2 (Anatase) Nanoparticles. *J. Phys. Chem. C* **2007**, *111* (40), 14925−14931.
(23) Kong, J.-Z.; Wang, S.-S.; Tai, G.-A.; Zhu, L.; Wang, L.-G.; Zhai, H.-F.; Wu, D.; Li, A.-D.; Li, H. Enhanced Electrochemical Performance of LiNi 0.5 Co 0.2 Mn 0.3 O 2 Cathode Material by Ultrathin ZrO 2 Coating. *J. Alloys Compd.* **2016**, *657*, 593−600.
(24) Yang, T.; Zhang, N.; Lang, Y.; Sun, K. Enhanced Rate Performance of Carbon-Coated LiNi0.5Mn1.5O4 Cathode Material for Lithium Ion Batteries. *Electrochim. Acta* **2011**, *56* (11), 4058−4064.

https://doi.org/10.1021/acsaem.5c00264
ACS Appl. Energy Mater. 2025, 8, 4941−4947